

LatexLens: An Interactive AI-Powered Annotation and Quantification Framework for Laticifers in Plant Microscopy

Sergio Madrid Pérez¹, Sofía Martínez Pastor¹, Francisco J. Escaray², Pablo Vera², Cèsar Ferri¹, Carlos Monserrat¹

¹Valencian Research Institute for Artificial Intelligence, Universitat Politècnica de València, València, Spain

²Instituto de Biología Molecular y Celular de Plantas, Universidad Politécnica de Valencia-Consejo Superior de Investigaciones Científicas, València, Spain

smadper@upv.edu.es, smarpas@ade.upv.es, fjescmaz@ibmcp.upv.es, vera@ibmcp.upv.es, cferri@dsic.upv.es, cmonserr@dsic.upv.es

Abstract

The analysis of laticifers in plant tissues is crucial for understanding latex production and plant defence mechanisms. However, the segmentation of these microscopic structures is hindered by their intricate topology, low contrast, and high-resolution imaging requirements. While Deep Learning models have shown promise, the gap between raw model inference and usable biological data remains significant due to the lack of accessible interfaces for domain experts. In this paper, we present LatexLens, a comprehensive desktop application built upon the napari ecosystem. The tool integrates a U-Net-based inference engine, domain-specific pre-processing (CLAHE), and a Human-in-the-Loop (HITL) workflow for mask refinement. Furthermore, we implement automated biological quantification directly within the GUI, focusing on metrics botanists use in practice: laticifer area fraction within the tissue and transect-based intersection counts that estimate network density. This focus bridges the gap between computer vision outputs and reproducible botanical measurements.

Demo Video: <https://youtu.be/iH57-hDS740>

1 Introduction

Laticifers are specialised internal secretory structures found in various plant species, responsible for the production and storage of latex [Fahn, 1979]. Understanding the morphology and distribution of these cells is essential for applications ranging from plant physiology to the industrial extraction of natural rubber and pharmaceutical compounds [Agrawal and Konno, 2009; Hagel *et al.*, 2008]. However, analysing these structures in microscopy images poses significant computer vision challenges. Laticifers often appear as thin, elongated, and anastomosing networks embedded within complex tissue backgrounds, often suffering from low contrast and noise.

Recent advancements in Deep Learning, particularly Convolutional Neural Networks (CNNs) [LeCun *et al.*, 1989],

such as U-Net [Ronneberger *et al.*, 2015], have revolutionised biomedical image segmentation. However, a persistent bottleneck in deploying these models is the lack of user-friendly interfaces that enable biologists to leverage these algorithms effectively. Furthermore, a segmentation mask itself is not the end goal; biological insights depend on derived calculations such as the laticifer area fraction within the image, and line-intersection counts that reflect cell density.

To address these challenges, we propose LatexLens, an interactive annotation and quantification tool. Built on the napari [Chiu *et al.*, 2022] multi-dimensional image viewer, our application provides a seamless workflow for:

- AI-Assisted Annotation:** Integrating pre-trained models for automated segmentation using tiling strategies.
- Preprocessing & Refinement:** Interactive image enhancement and mask editing tools.
- Biological Quantification:** Calculation of density and transect-based metrics essential for botanical analysis.
- Batch Processing:** Automated inference and metric extraction across full folders of images.

2 Data Acquisition and Dataset

The development and validation of our framework relied on a specialised dataset of plant microscopy images. The biological material corresponds to leaves of the species *Euphorbia lathyris* (caper spurge), genotype SY03, provided by the *Instituto de Biología Molecular y Celular de Plantas* (IBMCP).

2.1 Sample Preparation and Imaging

A standardised protocol was followed to ensure consistent image quality. Leaves were collected from the third or fourth node from the plant's apex. The basal third of each leaf was selected, and the abaxial epidermis was carefully removed (peeled) to expose the internal tissue structures. Samples were decolourised overnight in a methanol-acetone mixture and subsequently stained with 0.05% Ruthenium Red for 30 minutes to highlight pectins in cell walls and laticifers.

Imaging was performed using a Leica MZ16F *MacroFluo* fluorescence stereomicroscope with a GFP filter. The raw

75 output consisted of high-resolution single-channel fluores-
76 cence images where laticifers appear as bright, intercon-
77 nected structures against a darker background.

78 2.2 Dataset Characteristics

79 The complete dataset comprises 73 high-resolution images,
80 each with dimensions of 3840×2400 pixels.

- 81 • **Labeled Subset:** 35 images were manually annotated
82 by expert biologists. These ground truth masks delineate
83 the full extent of the laticifer network and were used for
84 supervised training of the model.
- 85 • **Unlabeled Subset:** An additional 38 images were pro-
86 vided without annotations.

87 Although the dataset contains 73 full-resolution leaves,
88 patch extraction substantially increases the number of train-
89 ing samples. With a tile size of 512×512 and overlap, each
90 image contributes many local patches, improving gradient di-
91 versity and helping the model learn fine laticifer patterns.

92 Several factors make this dataset particularly challenging
93 for automated analysis: (i) extreme class imbalance, as lati-
94 cifer pixels occupy only 4.6% of the total image area; (ii)
95 structural complexity, with thin, branching networks of vari-
96 able thickness requiring models to preserve topological con-
97 nectivity; and (iii) label noise, as the manual annotation diffi-
98 culty introduces inherent imperfections.

99 3 System Architecture

100 The system is designed as a modular desktop application us-
101 ing Python. The core architecture separates the User In-
102 terface (UI), the Deep Learning Inference Engine, and the
103 Data/Quantification logic.

104 3.1 Frontend and Interaction Layer

105 The frontend is built with qtpy and integrated as a dock wid-
106 get in napari, a fast, GPU-accelerated viewer for multidimen-
107 sional images. This choice allows for the rendering of large
108 microscopy images without performance degradation.

109 A central control widget serves as the primary hub, listen-
110 ing for layer insertion or removal to dynamically enable or
111 disable tools based on the current context (e.g., quantification
112 controls only activate once a mask layer exists).

113 3.2 Deep Learning Backend

114 The inference logic is decoupled from the UI to ensure re-
115 sponsiveness. We utilise PyTorch [Paszke *et al.*, 2019] for
116 the model backend.

117 The core segmentation model is built upon the U-Net ar-
118 chitecture [Ronneberger *et al.*, 2015]. To enhance feature ex-
119 traction capabilities, we employ an SE-ResNeXt-50 encoder
120 [Hu *et al.*, 2018]. This encoder is initialised with weights
121 pre-trained on the ImageNet dataset [Deng *et al.*, 2009], fa-
122 cilitating faster convergence and improved generalisation de-
123 spite the limited size of the botanical training dataset. Eval-
124 uated via 5-fold cross-validation, this configuration achieves
125 a connectivity-aware Dice (cIDice) [Shit *et al.*, 2021] of 0.58
126 and a standard Dice [Dice, 1945] of 0.49, ensuring robust
127 topological preservation for downstream quantification.

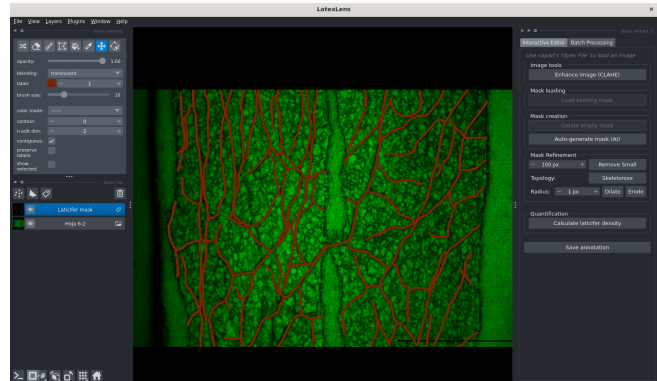


Figure 1: The LatexLens graphical user interface. The central panel displays the microscopy image with the AI-generated segmentation mask overlaid. The dock widget on the right provides controls for image enhancement, mask generation, refinement, and biological quantification settings.

Given the large dimensions of the input images, whole- 128
image inference is computationally infeasible on standard 129
GPUs. We implement a tiled inference strategy. The im- 130
age is padded to ensure divisibility by the patch size (default 131
 512×512). A sliding window with a defined stride (default 132
256) extracts patches. To mitigate edge artifacts common 133
in tiled inference, we employ an overlapping strategy where 134
predictions in overlapping regions are accumulated and aver- 135
aged. 136

137 4 Annotation Workflow

The application supports a complete pipeline, illustrated in 138
Figure 2, from image loading to the export of quantified data. 139

140 4.1 Preprocessing

Microscopy images often suffer from uneven illumination 141
and low contrast. We integrated an image enhancement mod- 142
ule directly into the UI. It utilises Contrast Limited Adaptive 143
Histogram Equalisation (CLAHE) [Pizer *et al.*, 1987]. 144

In the backend, the system automatically handles data type 145
conversion and channel reduction (RGB to Grayscale) before 146
applying CLAHE. For RGB data, the grayscale conversion 147
uses the green channel, matching the fluorescence signal used 148
in acquisition and avoiding channel mixing artefacts. 149

150 4.2 AI-Assisted Mask Generation

Users can trigger the “Auto-generate mask” function. This 151
calls the backend inference engine described in Section 3.2. 152
The resulting binary mask is injected into the viewer as a new 153
interactive label layer. Crucially, the layer is set to ‘editable’ 154
mode immediately. This supports a Human-in-the-Loop ap- 155
proach where the AI provides a “warm start” (often 80-90% 156
accurate), and the expert biologist corrects false positives 157
or connects broken laticifers using Napari’s built-in painting 158
tools. The main interface, displaying a segmented image and 159
the control widget, is shown in Figure 1. 160

4.3 Batch Processing

For large experiments, the system provides a batch-processing tab that accepts an input directory of microscopy images and outputs a mirrored directory of predicted masks. The batch pipeline performs tiled inference for each image and records per-image metrics into a CSV file. This feature enables researchers to process entire datasets without manual interaction while still preserving a structured audit trail.

4.4 Quantification Suite

A key contribution of this work is the integration of domain-specific biological metrics. Raw binary masks are insufficient for biological analysis; derived metrics are required. We implement two primary quantification methods:

Pixel Density Ratio

This metric calculates the area fraction occupied by laticifers:

$$D_{pixel} = \frac{\sum_{x,y} \mathbb{I}(M_{x,y} > 0)}{H \times W} \times 100 \quad (1)$$

where M is the segmentation mask. To avoid background bias when images contain surrounding black borders, the tool can automatically derive a tissue-only region from the laticifer network using a convex-hull [Graham, 1972] or morphological envelope, effectively cropping the measurement to the leaf area before computing density.

Transect Intersection Method

In stereology and plant anatomy, network density is often estimated by counting intersections with test lines (transects). We digitise this method within the quantification module. The user specifies the number of lines (N) and direction (horizontal/vertical/both). The system generates equidistant lines across the image. For each line L_i , we analyse the pixel intensity profile. An intersection is detected as a transition from background (0) to foreground (1).

$$Intersections(L_i) = \sum_j [P_j = 0 \wedge P_{j+1} = 1] \quad (2)$$

In this expression, L_i is the i -th transect line, P_j is the binary mask value sampled at position j along that transect, and the logical condition $[P_j = 0 \wedge P_{j+1} = 1]$ counts each background-to-laticifer transition as one intersection.

The application visualises these transects as vector shapes overlaid on the image and highlights intersection points. The statistics (mean intersections per line \pm std) are reported to the user and logged to the CSV.

5 Implementation Details

5.1 Handling High-Resolution Imagery

The GUI ensures thread safety when interacting with the viewer. To prevent memory overflows during inference on 4K resolution images, the sliding window approach processes tensors on the GPU and offloads accumulated results to CPU memory where necessary.

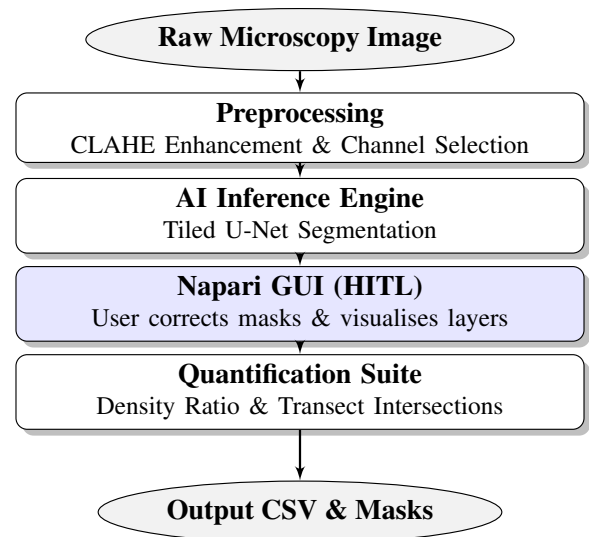


Figure 2: The Annotation Workflow. The system processes raw images through enhancement and AI segmentation before presenting them in the Napari interface. Users can interactively refine the masks (Human-in-the-Loop) before automated quantification.

5.2 Data Persistence

A dedicated persistence routine ensures data integrity and creates a robust audit trail for biological experiments. When the user presses the saving button, the system performs the following operations atomically:

1. Saves the original state of the image.
2. Saves the current state of the mask (potentially manually refined).
3. Recalculates all metrics (Density and Transect) based on the original image and the saved state of the mask.
4. Appends a row to a CSV log file with timestamps, dimensions, and computed metric.

6 Discussion and Future Work

We presented LatexLens, a tool that democratizes access to deep learning segmentation for plant biologists. By wrapping complex inference logic in a familiar GUI and integrating standard biological quantification metrics, we significantly reduce the time required for laticifer analysis.

The modular design allows for future extensions. Currently, the system uses a 2D U-Net. Future work includes integrating 3D segmentation capabilities for confocal microscopy stacks.

Acknowledgments

This work has been supported by CIPROM/2022/6 (FASS-LOW), funded by Generalitat Valenciana, and Spanish grant PID2024-162030OB-100 (ROBIN), funded by MCIN/AEI/10.13039/501100011033 and ERDF “A way of making Europe”, Cátedra ENIA-UPV in Sustainable AI Development, TSI-100930-2023-9.

References

- 235
236 [Agrawal and Konno, 2009] Anurag Agrawal and Kotaro
237 Konno. Latex: A model for understanding mechanisms,
238 ecology, and evolution of plant defense against herbivory.
239 *Annu. Rev. Ecol. Evol. Syst.*, 40:311–31, 12 2009.
- 240 [Chiu *et al.*, 2022] Chi-Li Chiu, Nathan Clack, and the na-
241 pari community. napari: a python multi-dimensional im-
242 age viewer platform for the research community. *Microscopy and Microanalysis*, 28(S1):1576–1577, 08 2022.
- 244 [Deng *et al.*, 2009] Jia Deng, Wei Dong, Richard Socher, Li-
245 Jia Li, Kai Li, and Li Fei-Fei. Imagenet: A large-scale
246 hierarchical image database. In *2009 IEEE Conference on*
247 *Computer Vision and Pattern Recognition*, pages 248–255,
248 2009.
- 249 [Dice, 1945] Lee R. Dice. Measures of the amount of eco-
250 logic association between species. *Ecology*, 26(3):297–
251 302, 1945.
- 252 [Fahn, 1979] Abraham Fahn. Secretory tissues in plants.
253 1979.
- 254 [Graham, 1972] Ronald L. Graham. An efficient algorithm
255 for determining the convex hull of a finite planar set. *Inf.*
256 *Process. Lett.*, 1:132–133, 1972.
- 257 [Hagel *et al.*, 2008] Jillian Hagel, Edward Yeung, and Peter
258 Facchini. Got milk? the secret life of laticifers. *Trends in*
259 *plant science*, 13:631–9, 11 2008.
- 260 [Hu *et al.*, 2018] Jie Hu, Li Shen, and Gang Sun. Squeeze-
261 and-excitation networks. In *Proceedings of the IEEE con-*
262 *ference on computer vision and pattern recognition*, pages
263 7132–7141, 2018.
- 264 [LeCun *et al.*, 1989] Y. LeCun, B. Boser, J. S. Denker,
265 D. Henderson, R. E. Howard, W. Hubbard, and L. D.
266 Jackel. Backpropagation applied to handwritten zip code
267 recognition. *Neural Computation*, 1(4):541–551, 1989.
- 268 [Paszke *et al.*, 2019] Adam Paszke, Sam Gross, Francisco
269 Massa, Adam Lerer, James Bradbury, Gregory Chanan,
270 Trevor Killeen, Zeming Lin, Natalia Gimelshein, Luca
271 Antiga, et al. Pytorch: An imperative style, high-
272 performance deep learning library. *Advances in neural in-*
273 *formation processing systems*, 32, 2019.
- 274 [Pizer *et al.*, 1987] Stephen M. Pizer, E. Philip Amburn,
275 John D. Austin, Robert Cromartie, Ari Geselowitz, Trey
276 Greer, Bart ter Haar Romeny, John B. Zimmerman, and
277 Karel Zuiderveld. Adaptive histogram equalization and its
278 variations. *Computer Vision, Graphics, and Image Pro-*
279 *cessing*, 39(3):355–368, 1987.
- 280 [Ronneberger *et al.*, 2015] Olaf Ronneberger, Philipp Fis-
281 cher, and Thomas Brox. U-net: Convolutional networks
282 for biomedical image segmentation. In Nassir Navab,
283 Joachim Hornegger, William M. Wells, and Alejandro F.
284 Frangi, editors, *Medical Image Computing and Computer-*
285 *Assisted Intervention – MICCAI 2015*, pages 234–241,
286 Cham, 2015. Springer International Publishing.
- 287 [Shit *et al.*, 2021] Suprosanna Shit, Johannes C. Paetzold,
288 Anjany Sekuboyina, Ivan Ezhov, Alexander Unger, An-
drey Zhyhka, Josien P.W. Pluim, Ulrich Bauer, and Bjo- 289
ern H. Menze. cIDice: A Novel Topology-Preserving Loss 290
Function for Tubular Structure Segmentation. In *Proc.* 291
IEEE/CVF Conference on Computer Vision and Pattern 292
Recognition (CVPR), pages 16560–16569, 2021. 293